Multiple Modes of Calcium-induced Calcium Release In Sympathetic Neurons II: A $[Ca^{2+}]_i$- and Location-dependent Transition from Endoplasmic Reticulum Ca Accumulation to Net Ca Release

Jarin Hongpaisan,[1] Natalia B. Pivovarova,[1] Stephen L. Colegrove,[3] Richard D. Leapman,[2] David D. Friel,[3] and S. Brian Andrews[1]

[1]Laboratory of Neurobiology, National Institute of Neurological Disorders and Stroke, and [2]Bioengineering and Physical Science Program, Office of the Director, National Institutes of Health, Bethesda, MD 20892

[3]Department of Neuroscience, Case Western Reserve University, Cleveland, OH 44106

ABSTRACT CICR from an intracellular store, here directly characterized as the ER, usually refers to net Ca^{2+} release that amplifies evoked elevations in cytosolic free calcium ($[Ca^{2+}]_i$). However, the companion paper (Albrecht, M.A., S.L. Colegrove, J. Hongpaisan, N.B. Pivovarova, S.B. Andrews, and D.D. Friel. 2001. *J. Gen. Physiol.* 118:83–100) shows that in sympathetic neurons, small $[Ca^{2+}]_i$ elevations evoked by weak depolarization stimulate ER Ca accumulation, but at a rate attenuated by activation of a ryanodine-sensitive CICR pathway. Here, we have measured depolarization-evoked changes in total ER Ca concentration ($[Ca]_{ER}$) as a function of $[Ca^{2+}]_i$, and found that progressively larger $[Ca^{2+}]_i$ elevations cause a graded transition from ER Ca accumulation to net release, consistent with the expression of multiple modes of CICR. $[Ca]_{ER}$ is relatively high at rest (12.8 ± 0.9 mmol/kg dry weight, mean ± SEM) and is reduced by thapsigargin or ryanodine (5.5 ± 0.7 and 4.7 ± 1.1 mmol/kg, respectively). $[Ca]_{ER}$ rises during weak depolarization (to 17.0 ± 1.6 mmol/kg over 120s, $[Ca^{2+}]_i$ less than ~350 nM), changes little in response to stronger depolarization (12.1 ± 1.1 mmol/kg, $[Ca^{2+}]_i$ ~700 nM), and declines (to 6.5 ± 1.0 mmol/kg) with larger $[Ca^{2+}]_i$ elevations (>1 μM) evoked by the same depolarization when mitochondrial Ca^{2+} uptake is inhibited (FCCP). Thus, net ER Ca^{2+} transport exhibits a biphasic dependence on $[Ca^{2+}]_i$. With mitochondrial Ca^{2+} uptake enabled, $[Ca]_{ER}$ rises after repolarization (to 16.6 ± 1.8 mmol/kg at 15 min) as $[Ca^{2+}]_i$ falls within the permissive range for ER Ca accumulation over a period lengthened by mitochondrial Ca^{2+} release. Finally, although spatially averaged $[Ca]_{ER}$ is unchanged during strong depolarization, net ER Ca^{2+} release still occurs, but only in the outermost ~5-μm cytoplasmic shell where $[Ca^{2+}]_i$ should reach its highest levels. Since mitochondrial Ca accumulation occurs preferentially in peripheral cytoplasm, as demonstrated here by electron energy loss Ca maps, the Ca content of ER and mitochondria exhibit reciprocal dependencies on proximity to sites of Ca^{2+} entry, possibly reflecting indirect mitochondrial regulation of ER Ca^{2+} transport.

KEY WORDS: calcium signaling • mitochondria • ryanodine • electron probe X-ray microanalysis • electron energy loss spectrum imaging

INTRODUCTION

Neurons respond to depolarizing stimuli with a rise in the concentration of free cytosolic calcium ($[Ca^{2+}]_i$). This rise, initiated by Ca^{2+} entry through voltage-gated channels, is strongly influenced by the activity of intracellular calcium stores (Pozzan et al., 1994; Berridge, 1998; Verkhratsky and Petersen, 1998). One important calcium store, operationally defined by its sensitivity to caffeine and ryanodine, is a locus for CICR. A large body of work in a variety of neurons indicates that CICR accelerates stimulus-evoked Ca^{2+} elevations (Kuba, 1994; Verkhratsky and Shmigol, 1996; Alonso et al., 1999; Emptage et al., 1999; Sandler and Barbara, 1999; Usachev and Thayer, 1999). In sympathetic neurons, evidence pointing to such a role for CICR comes from the effects of caffeine and ryanodine on stimulus-evoked $[Ca^{2+}]_i$ elevations and the supralinear dependence of these elevations on stimulus duration (Lipscombe et al., 1988; Thayer et al., 1988; Friel and Tsien, 1992; Kuba, 1994). As in other cells, CICR is thought to accelerate evoked $[Ca^{2+}]_i$ responses by promoting net Ca^{2+} release from the ER. However, we have presented evidence in the companion paper (see Albrecht et al., 2001, in this issue) for an alternative outcome during weak stimulation, namely, net Ca accumulation at a rate that is modulated by a Ca^{2+}-release pathway. In this case, the ER acts as a Ca^{2+} buffer, but one whose strength is downregulated by the activation of a $[Ca^{2+}]_i$-dependent, ryanodine-sensitive Ca^{2+} release pathway as $[Ca^{2+}]_i$ rises during stimulation.

In that study, a model was presented that describes the interplay between $[Ca^{2+}]_i$-dependent uptake and

Address correspondence to S.B. Andrews, Building 36, Room 2A-21, 36 Convent Drive, National Institutes of Health Bethesda, MD 20892-4062. Fax: (301) 480-1485; E-mail: sba@helix.nih.gov

release processes as the critical factor in determining the direction and rate of net ER Ca^{2+} transport. This model distinguishes three distinct "modes" of CICR; it accounts for Ca^{2+} buffering at low $[Ca^{2+}]_i$ (Mode 1), but also predicts that in certain cases buffering strength will be further attenuated, and eventually eliminated, by graded activation of the Ca^{2+} release pathway. If activation of the CICR pathway is sufficiently strong at high $[Ca^{2+}]_i$ that the rate of Ca^{2+} release can exceed the rate of uptake, stimulation should lead to net Ca^{2+} release. In one mode (moderate $[Ca^{2+}]_i$, Mode 2) the transition is gradual, whereas for the other (high $[Ca^{2+}]_i$, Mode 3) CICR may be regenerative, although both cases correspond to classical CICR and are expected to amplify depolarization-evoked $[Ca^{2+}]_i$ elevations in concert with a reduction in the Ca load of the ER.

The present study tests several predictions of this model by directly measuring changes in total calcium concentrations within the ER ($[Ca]_{ER}$) that occur in response to changes in $[Ca^{2+}]_i$ during depolarization and/or in the presence of agents that affect intracellular Ca^{2+} transport. A basic analysis of elemental composition and Ca^{2+}-handling characteristics confirmed that the ER is the structural correlate of the ryanodine-sensitive Ca^{2+} store. We then examined how $[Ca]_{ER}$ changes during and after steady depolarization as a function of $[Ca^{2+}]_i$, time, and intracellular location. The results show that as depolarization-induced increases in $[Ca^{2+}]_i$ become larger, there is a switchover from Ca^{2+} buffering to net Ca^{2+} release, providing direct experimental support for Mode 2 or 3 CICR in these cells. They also reveal a dependence of ER Ca^{2+} handling on radial position within the cell that is reciprocal to the described previously radial gradient of mitochondrial Ca content (Pivovarova et al., 1999a), the shape and magnitude of which is refined by calcium maps obtained from electron energy loss spectrum images.

MATERIALS AND METHODS

Cell Preparation and Measurement of $[Ca^{2+}]_i$

Preparations of bullfrog sympathetic neurons, as isolated cells in primary culture or as dispersed ganglia, were obtained as described previously (Pivovarova et al., 1999a; Colegrove et al., 2000); these papers also describe measurements of cytosolic free calcium concentrations ($[Ca^{2+}]_i$).

Measurement of $[Ca]_{ER}$

The concentration of total calcium within individual cisternae of ER ($[Ca]_{ER}$) was measured by energy-dispersive X-ray (EDX)* microanalysis of freeze-dried cryosections obtained from rapidly frozen dispersed ganglia, as described (Pivovarova et al., 1999a; see also Buchanan et al., 1993; Pozzo-Miller et al., 1997). Briefly, specimens were frozen at defined times and conditions by impact against a liquid nitrogen-cooled copper block using a modified CF-100 freezing machine (LifeCell). Cryosections (80-nm nominal thickness) were prepared from the well frozen specimen face by means of Leica Ultracut S/FCS or Ultracut E/FC-4E ultracryomicrotomes. Sections mounted on carbon- and Formvar-coated grids were cryotransferred into an analytical electron microscope (model EM912 Omega; LEO Electron Microscopy) or into an HB501 field-emission scanning transmission electron microscope (VG Instruments) and freeze-dried at about −110°C. EDX spectra were recorded at about −170°C in the LEO 912 Omega, which was equipped with a Linksystem Pentafet EDX detector (Oxford Instruments) and a ProScan slow-scan CCD camera controlled by AnalySIS software (Soft-Imaging Software GmbH). A nominal probe size of 63 nm was used; smaller probes yielded essentially similar results, confirming that the ~63-nm probe was adequate to determine ER content without significant contamination from adjacent cytosol. To avoid overlying cytosol, only cisternae wholly contained within the section were analyzed.

Depolarization-induced changes in $[Ca]_{ER}$ were measured by transferring ganglia from normal Ringer's to depolarizing media (30 K^+ or 50 K^+ Ringer's, isotonic substitution of Na^+) for times specified. For 10-s depolarizations, the solution change was accomplished by continuous superfusion on the stage of the freezing machine. Repolarization experiments were performed by transferring ganglia that had been depolarized for 2 min in 50 K^+ back to normal Ringer's for specified times. The effect of ryanodine was assayed by preincubating ganglia in normal Ringer's containing 1 μM ryanodine plus 10 mM caffeine for 5 min; the latter facilitates the use-dependent effects of ryanodine on the CICR store. For $[Ca]_{ER}$ measurements in unstimulated cells, ganglia were then transferred to normal Ringers plus 1 μM ryanodine without caffeine 1 min before rapid freezing. For measurements of depolarization-evoked $[Ca]_{ER}$ changes, ganglia were preincubated with caffeine plus ryanodine followed by ryanodine only as described, then transferred to high K^+ Ringer's plus ryanodine before rapid freezing.

Electron Energy Loss Spectrum Imaging

Spectrum images (EELSI's) are x-y arrays of pixels, i.e., images, containing a segment of an electron energy loss spectrum at every pixel. EELSI's were acquired using a Gatan model 766 DigiPEELS (parallel-detection electron energy loss spectrometer; Gatan, Inc.) mounted on the HB501 STEM, as described previously (Leapman and Rizzo, 1999). A cold-field emission source in this instrument provides a probe of diameter ~1 nm with a current of ~1 nA. The spectrometer was equipped with a 1024-channel photodiode array detector with a read-out noise of ~2 counts (rms; equivalent to ~20 fast electrons). Frozen-hydrated cryosections were transferred into the STEM at liquid nitrogen temperature and were freeze-dried at −100°C before recooling to −160°C for analysis. Annular dark-field images and EELS-images were recorded using a Gatan DigiScan acquisition system together with Digital Micrograph software (V3.3.1) running on a Power Macintosh 9600/233 computer that incorporated the Gatan spectrum-imaging package of Hunt et al. (1999). The system enables EELSI's to be acquired from specimen regions defined on an initially recorded dark-field image. This software also corrects for specimen drift by acquiring at given intervals a fast dark-field STEM image from a defined region of the specimen. Each successive image is cross-correlated with the previous one and the probe position is adjusted accordingly. Drift correction was applied at the end of each scan line. An acquisition time of 0.4 s per pixel

Abbreviations used in this paper: EDX, energy-dispersive X-ray; EELS, electron energy loss spectroscopy; FCCP, carbonyl cyanide *p*-(trifluoromethoxy)phenylhydrazone; $InsP_3$, D-*myo*-inositol-1,4,5-trisphosphate; RyR, ryanodine receptor; SERCA, sarco- and endoplasmic reticulum Ca ATPase; Tg, thapsigargin.

was selected, which gave typical image collection times of 10–20 min. The spectrum-images were corrected for read-out noise, dark-current, and channel-to-channel gain variation at each pixel.

Calcium and carbon maps were computed by fitting the background in a pre-edge window according to an inverse power law. The extrapolated background was subtracted from the post-edge window to obtain the integrated elemental signals for the Ca L_{23} and C K core-edges at each pixel in the image. Post-edge windows of width Δ = 10 eV (from 345 to 355 eV) for calcium and width Δ = 50 eV (from 285 to 335 eV) for carbon were selected. Pre-edge windows of similar width were selected to perform the background extrapolation. Atomic fractions of N_{Ca}/N_C were computed from the ratios of signal intensities I_{Ca}/I_C by dividing by the ratios of partial scattering cross-sections obtained from the Gatan EL/P program. The calcium concentrations in mmol/kg dry weight were obtained from the measured atomic fraction of N_{Ca}/N_C using the formula: $[Ca] = N_{Ca}/N_C \times 4.5 \times 10^4$ (Leapman et al., 1993). Values of the partial cross sections for the spectrometer collection semi-angle of 20 mrad were 5.96×10^3 barns for Ca (Δ = 10 eV) and 4.99×10^3 barns for C (Δ = 50 eV).

Data Analysis, Reagents, and Supplies

Population results are expressed as mean ± SEM. Statistical significance was assessed using a sequentially rejective Bonferroni procedure for multiple comparisons against a single control, FWE = 0.05 (Holm, 1979). Fura-2-AM was obtained from Molecular Probes. Unless otherwise stated, all reagents were obtained from Sigma-Aldrich, whereas electron microscopy supplies were obtained from EMS or Ted Pella.

RESULTS

Characterization of the Endoplasmic Reticulum as the Ryanodine-sensitive Calcium Storage Organelle

Sympathetic neurons express an abundant network of ER (Fig. 1). They also contain internal Ca stores that take up Ca^{2+} using sarco- and endoplasmic reticulum Ca ATPase (SERCA) pumps and release this ion mainly via a caffeine- and ryanodine-sensitive CICR pathway (Kuba and Nishi, 1976; Thayer et al., 1988; Friel and Tsien, 1992; Cseresnyés et al., 1997). It is generally presumed that these mechanisms for Ca^{2+} homeostasis are invested in the ER, in which case several testable predictions follow. First, the ER should contain Ca at a high concentration under resting conditions. Second, the concentration of intraluminal total Ca should be reduced by inhibiting the SERCA pump-dependent uptake pathway. Third, the concentration of Ca should be reduced by caffeine and/or ryanodine. Finally, conditions that favor Ca accumulation should lead to an increase in the Ca content of the store.

To test these predictions, changes in the mean total Ca concentration within the ER ($[Ca]_{ER}$) were measured by EDX microanalysis of rapidly frozen cells in isolated ganglia, in parallel with measurements of free cytosolic Ca^{2+} ($[Ca^{2+}]_i$) in fura-2–loaded cultured neurons. The first observation is that resting $[Ca]_{ER}$, spatially averaged over the cell soma, was notably high, 12.8 ± 0.9 mmol/kg dry weight (±SEM; equivalent to

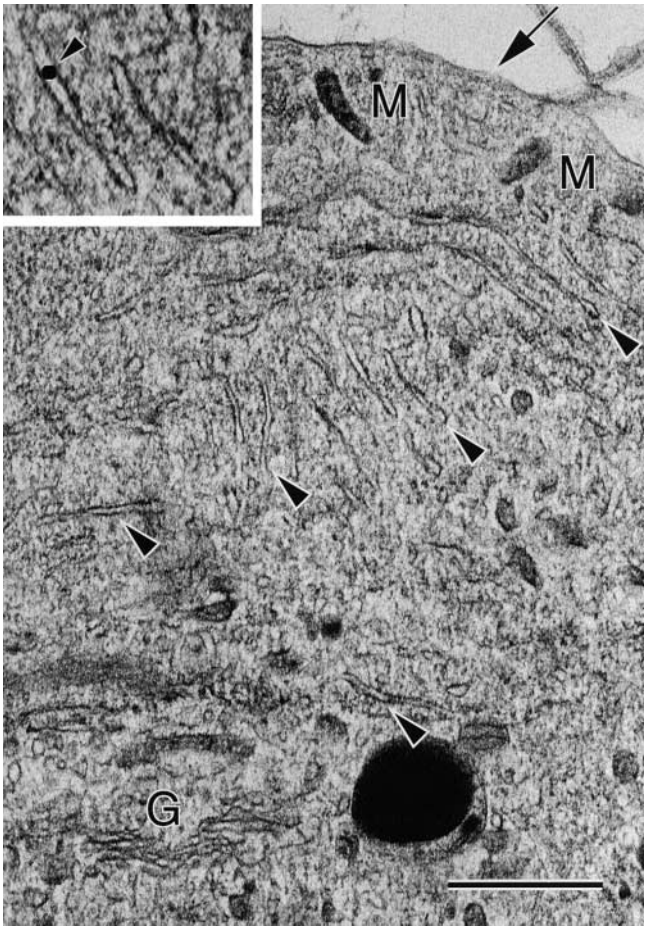

FIGURE 1. Subcellular structure and organization of sympathetic neurons. Digital dark-field scanning transmission electron micrograph (1024 × 1024 pixels) of freeze-dried cryosection prepared from a superficial neuron of an unfixed, rapidly frozen bullfrog sympathetic ganglion. Micrograph was recorded at about −170°C using low dose techniques. Field illustrates typical peripheral region of the neuronal soma (arrow indicates the plasma membrane) with a characteristic distribution of organelles. The cytoplasm contains a rich network of small tubules and cisternae of endoplasmic reticulum (arrowheads) and numerous mitochondria (M). A Golgi apparatus (G) is present in the perinuclear region, adjacent to large, dense spherical "inclusion body." (Inset) Enlargement of a pair of ER cisternae, showing the organelle lumen and membrane with stretches of attached ribosomes, illustrates the level of detail attainable in such preparations. Black dot indicates the relative size of nominal 63 nm-diam electron probe used for EDX analysis. Bar, 1,500 nm.

~3.6 ± 0.3 mmol/liter hydrated tissue; Table I, Fig. 2 A; see Pozzo-Miller et al., 1997 and Pivovarova et al., 1999a for an explanation of the concentration unit mmol/kg dry weight, and how to convert it to mmol/liter hydrated tissue). This value is higher than in any other organelle or compartment, including the cytoplasm (3.3 ± 1.0 mmol/kg dry weight). A second set of measurements showed that inhibiting Ca^{2+} uptake with Tg (1 μM) significantly reduced $[Ca]_{ER}$ (Table I and Fig. 2 A), consistent with the observation that Tg elicits a transient rise

TABLE I

Elemental Concentrations in the ER of Frog Sympathetic Neurons

	n	Na	Mg	P	K	Ca
				mmol/kg dry weight		
Experimental condition						
Control	111	28 ± 9	39 ± 2	611 ± 17	673 ± 14	12.8 ± 0.9
Thapsigargin	82	27 ± 4	29 ± 1	589 ± 17	562 ± 15	5.5 ± 0.7[a]
Ryanodine (caffeine preincubation)	59	25 ± 5	30 ± 2	583 ± 16	590 ± 18	4.7 ± 1.1[a]
30 mM K^+ (2 min)	66	31 ± 4	37 ± 4	651 ± 28	656 ± 31	17.0 ± 1.6[a]
30 mM K^+ (45 s)	61	23 ± 5	25 ± 2	573 ±16	601 ± 18	11.8 ± 1.1
30 mM K^+ (45 s) + thapsigargin	94	38 ± 4	33 ± 3	577 ± 14	626 ± 16	7.8 ± 1.0
30 mM K^+ (45 s) + ryanodine	80	23 ± 2	30 ± 2	628 ± 10	606 ± 11	9.9 ± 0.9[b]
50 mM K^+ (10 s)	43	9 ± 2	34 ± 2	560 ± 16	578 ± 13	10.3 ± 0.9
50 mM K^+ (45 s)	60	17 ± 1	32 ± 3	593 ± 19	546 ± 20	11.5 ± 1.2
50 mM K^+ (2 min)	90	23 ± 2	28 ± 2	483 ± 18	475 ± 17	12.1 ± 1.1
50 mM K^+ (2 min) + recovery (5 min)	33	34 ± 7	32 ± 5	594 ± 26	616 ± 26	16.3 ± 2.2[a]
50 mM K^+ (2 min) + recovery (15 min)	37	33 ± 1	39 ± 5	636 ± 26	659 ± 26	16.6 ± 1.8[a]

Data are given as mean ± SEM, where column *n* is the number of ER cisternae analyzed. The number of neurons analyzed was 4–15 per experimental condition, taken from 2–5 ganglia. Concentrations were also obtained for sulfur and chlorine; for these elements, there were no significant concentration differences between locations or conditions.

[a]Significantly different from control ($P < 0.05$) as determined using a sequentially rejective Bonferroni procedure for multiple comparisons with FWE = 0.05 (see MATERIALS AND METHODS).

[b]Significantly different from matching treatment without depolarization (line 3, ryanodine (caffeine preincubation)) using *t* test, $P < 0.001$.

in $[Ca^{2+}]_i$ (Fig. 2 B), even in the absence of extracellular Ca^{2+} (not shown). Additional experiments indicated that RyR activation stimulated net Ca^{2+} release from the ryanodine-sensitive store. Thus, exposure first to ryanodine plus caffeine and then briefly to ryanodine alone reduced $[Ca]_{ER}$ (Table I and Fig. 2 A, Ryan, and Fig. 2 C) to similar levels as did Tg. Finally, sympathetic ER can, as a consequence of Ca^{2+} entry across the plasma membrane, accumulate Ca above basal levels; for example, $[Ca]_{ER}$ is elevated to 17.0 ± 1.6 mmol/kg dry weight by weak depolarization that raises $[Ca^{2+}]_i$ to ~300 nM (30 mM K^+ for 2 min; Table I; see Fig. 3 in Albrecht et al., 2001, in this issue). No other cellular compartment, including the mitochondria, Golgi apparatus, or nucleus, was affected by these drug treatments (not shown). Thus, the ER and only the ER had the pharmacological signature of the CICR pool.

These results identify the ER as the principal, probably the only, Ca store responsible for CICR, but leave open the question of whether the ER Ca pool is a single, homogeneous functional entity. Arguments based on the effects of ryanodine on basal Ca^{2+} uptake rates and supporting a single pool model were presented in the companion paper (see Albrecht et al., 2001, in this issue). Here, additional support comes from the observation that the distributions of $[Ca]_{ER}$ measurements from individual ER cisternae are normal under conditions of rest and depletion (Fig. 2, A and B, insets). Although there is a measurable inositol trisphosphate ($InsP_3$)-gated Ca^{2+} release pathway in amphibian sympathetic neurons (Pfaffinger et al., 1988), the lack of evidence for discreet pools may reflect the comparatively small size of this pool. Alternatively, it may indicate that the ryanodine- and $InsP_3$-sensitive pools are coextensive, or at least in functional communication, so that manipulating one pool affects the other.

A $[Ca^{2+}]_i$-dependent Transition from ER Ca Accumulation to Net Ca Release

In the companion paper (see Albrecht et al., 2001, in this issue), we presented evidence that during weak depolarization the ER accumulates Ca^{2+}, but net accumulation is opposed, and therefore attenuated, by activation of a Ca^{2+}- and ryanodine-sensitive Ca^{2+} release pathway. A predicted property for two of the three general types of CICR discussed in that study is a transition from Ca^{2+}-dependent Ca accumulation to net Ca^{2+} release—a change in the direction of net ER Ca^{2+} transport—as stimulus-evoked $[Ca^{2+}]_i$ elevations become larger. To determine if such a transition occurs, we examined changes in $[Ca]_{ER}$ induced by stimuli that increase $[Ca^{2+}]_i$ to higher levels. Isolated sympathetic ganglia were exposed to a various high K^+ Ringers' solutions for defined periods of time before rapid freez-

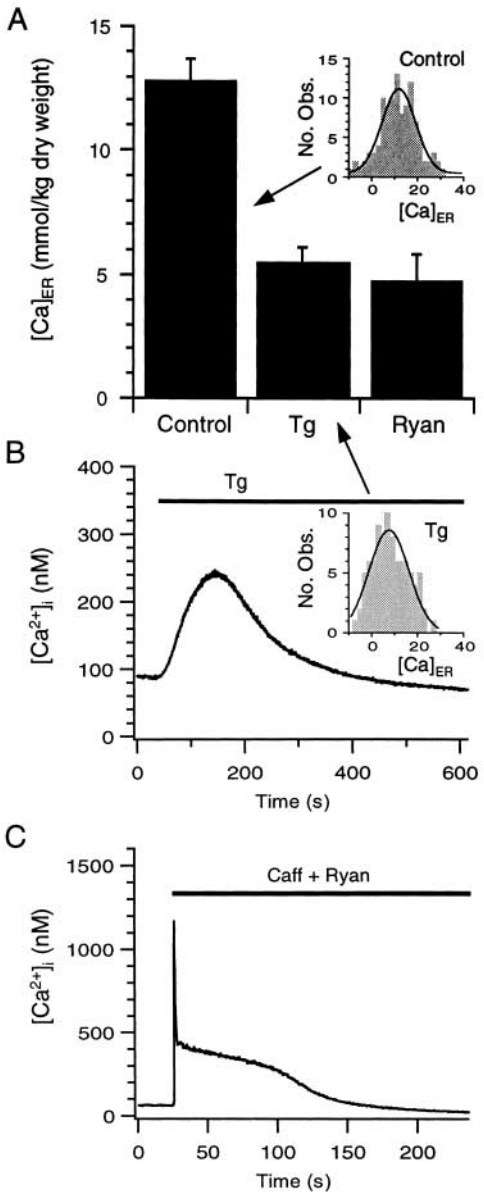

FIGURE 2. The ryanodine-sensitive Ca^{2+} store is the ER. The total Ca content of the ER in resting, untreated neurons is high (A, left bar). Treatment with thapsigargin (Tg) leads to a transient release of Ca^{2+} into the cytosol, as measured in the presence of 250 nM Tg in fura-2–loaded isolated neurons (B); in parallel experiments, SERCA pump inhibition by 1 μM Tg in dispersed ganglia leads to a reduction in $[Ca]_{ER}$ (A, $P < 0.0001$). Treatments that open the RyR channel—in this case, 5 min in the presence of 1 μM ryanodine plus 10 mM caffeine followed by 1 min in ryanodine only—deplete $[Ca]_{ER}$ as effectively (A, $P < 0.0001$), also in association with a cytosolic Ca^{2+} transient (C). (This transient was elicited by 10 mM caffeine in the continued presence of 1 μM ryanodine, applied 2 min before caffeine.) Note the long-lived (>1 min) plateau that follows the initial caffeine-mediated spike. This plateau, not seen in the Tg trace, is presumably indicative of active mitochondrial Ca^{2+} release after accumulation induced by earlier Ca^{2+} release from the ER. Error bars are ±SEM. (insets) Frequency distributions of individual $[Ca]_{ER}$ measurements for same data from control and Tg-treated cells (A and B, respectively) as in A (arrows)and Table I (distribution for ryanodine-treated cells was similar). Distributions are normal with SDs of best-fit Gaussians that are not significantly different ($\sigma = 10.4 \pm 1.1$ [Control] vs. 12.3 ± 0.9 [Tg]), consistent with the assumption that the ER can be treated as a single functional compartment.

ing and EDX analysis; $[Ca^{2+}]_i$ was determined in fura-2–loaded, isolated cells in parallel experiments.

Fig. 3 A illustrates a typical $[Ca^{2+}]_i$ response to strong depolarization (50 mM K^+, 2 min) elicited in the absence of drugs or CICR modifiers. During depolarization, $[Ca^{2+}]_i$ rapidly rises to a peak and declines toward a steady level of ~600–800 nM that is sustained for several minutes. Under these conditions, mitochondria avidly and continuously accumulate Ca (Pivovarova et al., 1999a), but $[Ca]_{ER}$ does not change significantly at either 45 s or 2 min (Fig. 3 D, middle data points and Table I). This finding is in contrast to the increase in $[Ca]_{ER}$ induced when $[Ca^{2+}]_i$ is ~300 nM under otherwise equivalent conditions (Fig. 3 D, top left data point). One interpretation is that although both Ca^{2+}-dependent Ca^{2+} uptake and release by the ER are accelerated when $[Ca^{2+}]_i$ reaches ~700 nM, the average rates of these processes are equal. In effect, the ER is cycling Ca^{2+}, i.e., "spinning its wheels."

In contrast to untreated cells, cells depolarized in the presence of 1 μM FCCP attain $[Ca^{2+}]_i$ levels in excess of 1 μM for ~1 min before undergoing a rapid decay to a steady, low level of ~200–300 nM (Fig. 3 B). After repolarization, $[Ca^{2+}]_i$ recovers to its prestimulus level with a plateau phase that is greatly reduced compared with the plateau observed under control conditions. The larger $[Ca^{2+}]_i$ response and the more rapid recovery are both consistent with suppression of mitochondrial Ca^{2+} uptake. Quite strikingly, depolarization in the presence of FCCP (45 s) reduces $[Ca]_{ER}$ to 6.5 ± 1.0 mmol/kg (Fig. 3 D, bottom right data point), showing that when $[Ca^{2+}]_i$ is very high, the ER loses net Ca. Net ER Ca^{2+} release would also explain the time course of $[Ca^{2+}]_i$, especially the >1-min-long "hump" (Fig. 3, compare B with C) seen under these conditions. The hump consists of a prolonged $[Ca^{2+}]_i$ elevation followed by a rapid decline (at arrow, Fig. 3 B). In cells treated with Tg, in addition to FCCP, the hump is not observed, consistent with the idea that it reflects net Ca^{2+} release from the ER. The basis for the accelerated recovery after ~2 min of FCCP exposure is not known, but, regardless of specific mechanisms, the prompt return to normal resting $[Ca^{2+}]_i$ levels after repolarization indicates that exposure to FCCP had not depleted ATP sufficiently to affect normal Ca^{2+} clearance mechanisms; if it had, a return to a much higher basal $[Ca^{2+}]_i$ level would be expected.

To summarize, there is a biphasic relationship between the $[Ca^{2+}]_i$ levels reached during depolarization

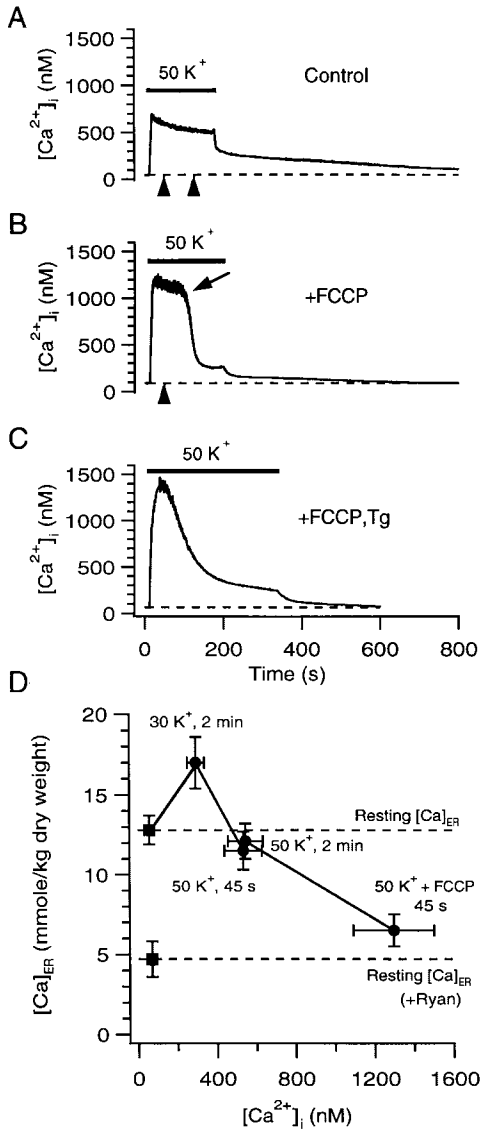

FIGURE 3. Biphasic changes in the calcium content of the ER as stimuli-evoked steady-state $[Ca^{2+}]_i$ increases. A-C: Fura-2 recordings of $[Ca^{2+}]_i$ changes during and after exposure to 50 mM K^+ under control conditions (A) and in the continuous presence of FCCP (1 μM) with (B) and without (C) functional SERCA pumps. Even with long (3 min) depolarizations, $[Ca^{2+}]_i$ in control cells (A) underwent a sustained elevation to >500 nM during depolarization, followed by a long plateau after repolarization that is attributable to mitochondrial Ca^{2+} release. Arrowheads indicate 45 s (A and B) and 2 min (A only) time points corresponding to data in D. Arrow on B indicates the "hump" discussed in RESULTS. To inhibit SERCA activity, cells were pretreated with Tg (200 nM) for 10 min, but were not exposed to Tg during recordings. (D) A plot of $[Ca]_{ER}$ versus $[Ca^{2+}]_i$ illustrates the biphasic relationship between these parameters, such that different stimulus conditions can lead to an increase, no change, or a decrease in $[Ca]_{ER}$. Dotted lines indicate $[Ca]_{ER}$ measured in resting cells in the absence and presence of caffeine plus ryanodine (Table I). The latter is the lowest value of $[Ca]_{ER}$ measured so far, and therefore defines the upper limit of minimum $[Ca]_{ER}$. Mobilizable ER Ca is significantly discharged at short times after strong depolarization in the presence of FCCP, a condition during which the absence of mitochondrial Ca^{2+} uptake, as well as enhanced net Ca^{2+} release, drives $[Ca^{2+}]_i$ to extremely high levels, *e.g.*, 1296 ± 204 nM in one representative cell. Error bars are ±SEM.

and parallel changes in $[Ca]_{ER}$ (Fig. 3 D). Increasing $[Ca^{2+}]_i$ from basal levels to ~300 nM leads to ER Ca accumulation, whereas with larger $[Ca^{2+}]_i$ elevations, $[Ca]_{ER}$ declines. To this point, the evidence for this relationship at high $[Ca^{2+}]_i$ depends on measurements obtained while FCCP was present for the purpose of inhibiting mitochondrial Ca^{2+} uptake. FCCP is generally thought to be a highly specific protonophore without short-term effects on mitochondrial structure at the concentration and exposure times used here (Stout et al., 1998; Minamikawa et al., 1999), although uncouplers have been reported to promote mitochondrial swelling under some circumstances (Garlid and Nakashima, 1983; Petronilli et al., 1993). However, we did not observe such effects and independent evidence for net ER Ca^{2+} release at high $[Ca^{2+}]_i$, obtained under conditions of intact Ca^{2+} homeostasis and presented below, argues against the possibility that the $[Ca]_{ER}$ reduction illustrated in Fig. 3 D is an indirect effect of inhibiting mitochondrial function.

Time Course of Stimulus-evoked Changes in $[Ca]_{ER}$ at Intermediate $[Ca^{2+}]_i$ Levels

Results just presented support the idea that with increasing $[Ca^{2+}]_i$, ER Ca accumulation slows, leading to lower and eventually to no net accumulation as Ca^{2+}

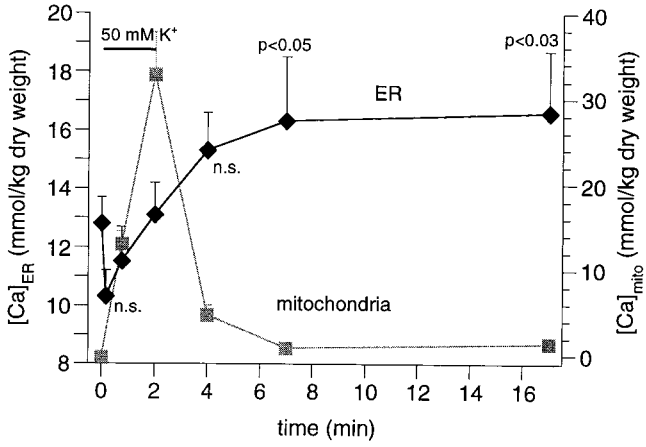

Figure 4. Comparative time courses of Ca^{2+} transport by ER and mitochondria. Comparison between the time courses of spatially averaged $[Ca]_{ER}$ (solid trace) and $[Ca]_{mito}$ (gray trace) reveals the reciprocal response of these organelles to strong depolarization (50 mM K^+, $[Ca^{2+}]_i$ ~600–800 nM). Whereas $[Ca]_{mito}$ increases monotonically during depolarization, as previously reported (Pivovarova et al., 1999a), globally averaged $[Ca]_{ER}$ remains essentially constant. (The apparent decline in $[Ca]_{ER}$ at 10 and 45 s after depolarization is not statistically significant.) After repolarization (from 2-min depolarizations), however, $[Ca]_{ER}$ increases, with a time course that parallels the prolonged $[Ca^{2+}]_i$ plateau that occurs during periods of mitochondrial Ca^{2+} release. The Ca load of the ER has a long lifetime, showing little sign of depletion for at least 15 min after repolarization. Each data point is the collected result (mean ± SEM) from several experiments; *n* (for individual organelles) was typically 50–100 (Table I). n.s. indicates not significant, but with $P < 0.1$. Error bars are ±SEM.

uptake and release come into balance. The finding that such a steady-state condition occurs when $[Ca^{2+}]_i$ is ~600 nM (Fig. 3 D) is further reinforced in Fig. 4, a plot of $[Ca]_{ER}$ as a function of time during and after strong depolarization, which shows that $[Ca]_{ER}$ changes little if at all during maintained strong depolarization. (The apparent, statistically insignificant decline at 10 s is discussed below). This behavior contrasts with the very large increases in the concentration of total mitochondrial Ca ($[Ca]_{mito}$) that occur under the same conditions (Fig. 4; Pivovarova et al., 1999a).

Upon repolarization, intracellular Ca^{2+} dynamics change dramatically as $[Ca^{2+}]_i$ recovers. How does $[Ca]_{ER}$ respond during this recovery phase? After repolarization (from 50 mM K^+, 2-min depolarization), $[Ca^{2+}]_i$ recovers in several kinetically distinct phases, the first two of which are strongly influenced by mitochondrial Ca^{2+} transport. The earliest phase is speeded by mitochondrial Ca accumulation, whereas the long second phase is slowed by net mitochondrial Ca^{2+} release (Fig. 3 A; Colegrove et al., 2000). During the second phase, when mitochondria actively extrude Ca^{2+} via the Na^+/Ca^{2+} exchanger, $[Ca^{2+}]_i$ is "clamped" at ~200–300 nM (Fig. 3 A) while $[Ca]_{mito}$ declines (Fig. 4, 2–7 min). Over this same period of the recovery, $[Ca]_{ER}$ rises significantly (Fig. 4), which is consistent with the $[Ca]_{ER}$ rise observed when $[Ca^{2+}]_i$ is within this same range during steady weak depolarization (see Albrecht et al., 2001, in this issue).

Fig. 4 also shows that $[Ca]_{ER}$ is elevated for >10 min after repolarization-induced loading. Average $[Ca]_{ER}$ in many cells has begun to decline by 15 min, although that is not evident in Fig. 4, owing to substantial cell–cell variability (which also accounts for the large error bars at 7 and 17 min). In any case, $[Ca]_{ER}$ recovers quite slowly. Presumably, this reflects a relatively small imbalance between the rates of ER Ca^{2+} uptake and release, as well as potentially slow rates of release at low $[Ca^{2+}]_i$, both factors contributing to the slow tail phase of $[Ca^{2+}]_i$ recovery that outlasts the period of mitochondrial Ca^{2+} release (Fig. 3 A). These observations are reminiscent of similar findings for the ER in these and other neurons (Shmigol et al., 1994a; Friel, 1995; Garaschuk et al., 1997; Pozzo-Miller et al., 1997) and suggests that long-lived Ca loads, carrying a "memory" of activity-evoked changes in $[Ca^{2+}]_i$, may be a general feature of neuronal ER.

Spatial Dependence of Depolarization-evoked Changes in $[Ca]_{ER}$ and Its Relationship to Mitochondrial Ca^{2+} Uptake

The results presented so far indicate that the ER accumulates Ca at low $[Ca^{2+}]_i$, releases net Ca^{2+} at high $[Ca^{2+}]_i$, and transports little net Ca^{2+} at intermediate levels. These conclusions are based on spatially averaged measurements of $[Ca]_{ER}$ from multiple cells after steady depolarizations that were much longer than necessary for decay of the initially large, stimulus-evoked radial $[Ca^{2+}]_i$ gradients, which dissipate in only a few seconds in these cells (Hernandez-Cruz et al., 1990; Hua et al., 1993b). During strong depolarization that raises $[Ca^{2+}]_i$ to ~600–800 nM, such measurements do not detect significant changes in average $[Ca]_{ER}$, but there is a tendency for (averaged) $[Ca]_{ER}$ to become lower as the length of depolarization shortens (Fig. 4). Therefore, we considered factors that might quantitatively depress spatially averaged $[Ca]_{ER}$ at short depolarization times. One potential contribution is spatial nonuniformity of $[Ca^{2+}]_i$ during initial periods of Ca^{2+} entry. We have provided evidence for the existence of radial gradients in the concentration of mitochondrial total Ca ($[Ca]_{mito}$) after long depolarization times (e.g., 45 s), and proposed that mitochondria maintain a record of previous, spatially heterogeneous $[Ca^{2+}]_i$, signals when the stimulus raises $[Ca^{2+}]_i$, high enough that mitochondria are forced into their so-called "buffering mode," thereby accumulating Ca continuously (Pivovarova et al., 1999a). Therefore, we asked if $[Ca]_{ER}$ might similarly provide a record of radial $[Ca^{2+}]_i$, gradients, one that conforms to the $[Ca^{2+}]_i$ dependence of ER Ca^{2+} transport.

An analysis of $[Ca]_{ER}$ as a function of distance from the plasma membrane in cells depolarized briefly (10 s) with 50 mM K^+ reveals that net Ca^{2+} release does in fact occur, but only in the outermost 5-μm shell of cytoplasm (Fig. 5 A). One likely explanation for this $[Ca]_{ER}$ gradient is that it reflects the transient radial gradients in $[Ca^{2+}]_i$ that arise from Ca^{2+} entry through voltage-sensitive Ca^{2+} channels during the initial seconds of depolarization (Hua et al., 1993b). During this period, $[Ca^{2+}]_i$ would reach its highest levels in the outermost cytoplasmic shells, after which channel inactivation would reduce Ca^{2+} entry and $[Ca^{2+}]_i$ gradients would dissipate by diffusion. Since $[Ca^{2+}]_i$ in the more interior shells would not exceed the equilibrium spatial average, which is ~600–800 nM in this case, $[Ca]_{ER}$ in these shells would change little, as observed. Furthermore, the dominance of these shells in the spatially averaged $[Ca]_{ER}$ values would largely obscure any local decline of $[Ca]_{ER}$ within peripheral cisternae (Fig. 4).

According to this general idea, radial $[Ca^{2+}]_i$ gradients drive spatial heterogeneities of $[Ca]_{ER}$, which, therefore, should be increasingly prominent as the strength of depolarization increases. In addition, for a stimulus of given strength, gradients would be most pronounced during the initial moments of stimulation. As $[Ca^{2+}]_i$ gradients dissipate, $[Ca]_{ER}$ would relax, independently of location, toward a value that depends on (now spatially uniform) $[Ca^{2+}]_i$. In contrast, such a relaxation would not occur for $[Ca]_{mito}$ if $[Ca^{2+}]_i$ remained above the level where mitochondria continuously accumulate Ca^{2+}. Thus, it appears that different regimes of CICR can coexist in different parts of the cell at a given time, with consequent effects on the direction of net Ca^{2+}

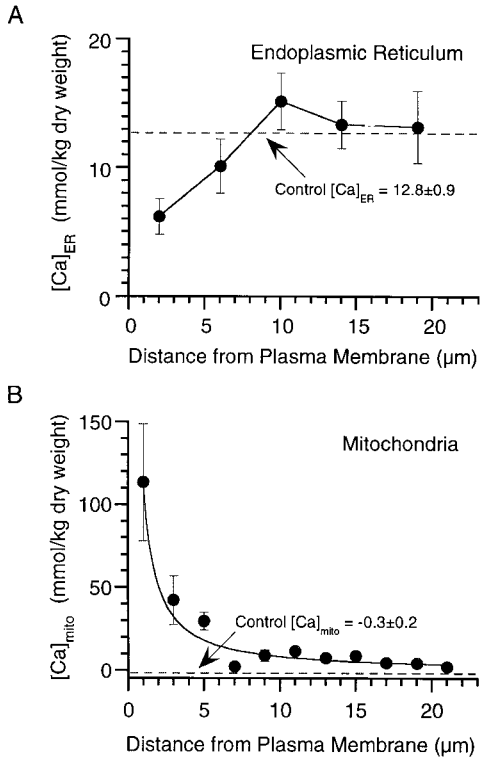

FIGURE 5. Radial spatial gradients of ER and mitochondrial calcium concentrations. ER and Mitochondria respond to depolarization-evoked Ca^{2+} influx with spatially complementary Ca^{2+} release and uptake, respectively. At short times (<1 min) after depolarization, these responses occur almost exclusively within the peripheral ~5 μm-wide cytoplasmic shell. (A) ER spatial profile at 10 s after strong depolarization is calculated from 109 individual EDX measurements, essentially as described (Pivovarova et al., 1999a). Data were binned into 4-μm shells. Only the outermost shell centered at 2 μm is significantly different from $[Ca]_{ER}$ of control neurons (assumed to be spatially uniform, as indicated by horizontal dotted line, 12.8 ± 0.9 mmol/kg dry weight). (B) Mitochondrial spatial profile at 45 s after strong depolarization (50 K^+) is derived from electron energy loss spectrum images (EELSI's; 40 separate images containing 113 mitochondria; see MATERIALS AND METHODS for details). $[Ca]_{mito}$ values are binned into 2-μm shells. Values for single mitochondria are spatially averaged over the matrix, and therefore resistant to microheterogeneity induced scatter. All $[Ca]_{mito}$ values except those bins centered at 7 and 21 μm are significantly higher ($P < 0.01$) than for spatially uniform $[Ca]_{mito}$ of control neurons (horizontal line, −0.3 ± 0.2 mmol/kg). Profile is comparable to that described previously on the basis of EDX measurements (Pivovarova et al., 1999a), but much more refined. Curve fit is a best-fit power function ($y \propto x^{-1.1}$). The form of this curve is similar to the diffusion model presented previously, except that $[Ca]_{mito}$ rises much more steeply near the plasma membrane; presumably, additional factors that accelerate mitochondrial Ca^{2+} uptake remain to be determined. Error bars are ±SEM.

transport. Viewed another way, the radial gradient of $[Ca]_{ER}$ observed after short depolarization recapitulates in a single cell the $[Ca^{2+}]_i$ dependence of CICR first deduced from spatially averaged $[Ca^{2+}]_i$ measurements after long depolarizations in cell populations (Fig. 3 D).

Mitochondria as Sensors of Subplasma Membrane $[Ca^{2+}]_i$ Gradients

We have previously reported that mitochondria within a similarly sized ~5-μm peripheral shell of cytoplasm accumulate disproportionately large amounts of Ca (Pivovarova et al., 1999a), and suggested that the resulting radial $[Ca]_{mito}$ gradient follows from differences in local $[Ca^{2+}]_i$ to which central and peripheral mitochondria are exposed during the history of stimulation. Modeling studies are consistent with this idea, and suggest that mitochondria, owing to the steep $[Ca^{2+}]_i$ dependence and integrative nature of mitochondrial Ca^{2+} transport, should serve as highly sensitive detectors of spatial nonuniformities in $[Ca^{2+}]_i$. However, the precision of the $[Ca]_{mito}$ measurements supporting these conclusions was limited by the punctate nature of mitochondrial Ca sequestration. Specifically, we and others (David, 1999; Pivovarova et al., 1999a,b) have reported preliminary evidence that evoked mitochondrial Ca^{2+} uptake leads to the transient formation of mainly small (<20 nm) calcium- and phosphorus-rich inclusions within the mitochondrial matrix. It has been speculated that these inclusions reflect a high capacity, chemical mechanism of mitochondrial Ca sequestration, but, regardless, their formation results in substantial heterogeneity in the distribution of intramitochondrial Ca, and therefore also to scatter for EDX point-probe analyses.

Here, we have applied a novel analytical approach—electron energy loss spectrum imaging (EELSI; Leapman et al., 1994)—that largely overcomes this difficulty because it comprehensively maps elemental distributions at better than 20-nm resolution (Leapman and Rizzo, 1999). To generate an EELSI, a high resolution EELS spectrum, with its inherently high Ca sensitivity, is acquired at every pixel over a selected field. Major advantages are that the specimen is exhaustively sampled, with an energy loss spectrum at each pixel that is suitable for rigorous quantitation. As a result, EELSI can detect microheterogeneity at the single pixel level, and provide a dataset suitable for determining the shape and magnitude of the depolarization-induced $[Ca]_{mito}$ gradient with much improved resolution and precision. The refined radial gradient for $[Ca]_{mito}$ (Fig. 5 B, compare Fig. 8 in Pivovarova et al., 1999a) was determined after stimulation of the same strength and duration (50 mM K^+, 45 s) used previously; qualitatively similar gradients can be detected as early as 10 s after depolarization. The results are consistent with the idea that radial $[Ca^{2+}]_i$ gradients lead to differences in the rate of mitochondrial Ca accumulation and, therefore, to the mitochondrial Ca load, and thus provide additional evidence that peripheral ER are exposed to a significant, spatially heterogeneous $[Ca^{2+}]_i$ signal. Finally, it is clear (the time difference between Fig. 5, A and B notwithstanding) that the gradient in $[Ca]_{mito}$ is reciprocal to

that for $[Ca]_{ER}$. Therefore, the spatial distribution of ER Ca^{2+} release, like the temporal distribution of Ca^{2+} uptake, is reciprocal and complementary to that of mitochondrial Ca^{2+} transport.

DISCUSSION

The goal of this study was to characterize the functional contributions of the ryanodine-sensitive Ca store to depolarization-evoked changes in $[Ca^{2+}]_i$, with a particular eye toward determining whether in sympathetic neurons this store acts as a Ca^{2+} source or as a sink. The study was prompted by our seemingly paradoxical observation that, although this store exhibits many of the hallmarks of classical CICR (Kuba, 1994; Verkhratsky and Shmigol, 1996; Usachev and Thayer, 1999), under conditions of weak depolarization, it actually accumulates Ca and slows evoked $[Ca^{2+}]_i$ elevations (Albrecht et al., 2001). Therefore, we extended those studies to include larger evoked $[Ca^{2+}]_i$ elevations, and find that although the ER is a graded Ca^{2+} buffer over the lower range of $[Ca^{2+}]_i$, progressive $[Ca^{2+}]_i$-dependent activation of its Ca^{2+} release pathway leads to weaker buffering, followed by a transition to net Ca^{2+} release, until finally the ER becomes a triggered Ca^{2+} source at high $[Ca^{2+}]_i$. These findings provide a conceptual framework for understanding previous studies of ER Ca^{2+} handling in these and other cells (Friel and Tsien, 1992; Hua et al., 1993a; Shmigol et al., 1995).

The ER Is the Structural Correlate of the Ryanodine-sensitive Ca Store

Since an important aspect of our approach depended on directly measuring changes in the Ca content of the ryanodine-sensitive store, it was necessary to know the corresponding subcellular structure. The Ca content of the ER ($[Ca]_{ER}$), as well as its pharmacological profile, directly identifies the ER as the principal, if not the only, structural correlate of this Ca store. Although this result is not surprising, it was essential to demonstrate, considering that other organelles may function as Ca stores (Verkhratsky and Petersen, 1998). Furthermore, even if the identity of the store is taken for granted, the amount of Ca it sequesters is critical for understanding the magnitude and direction of CICR. Note that other functions for the ER, such as $InsP_3$-gated Ca^{2+} release, spatially segregated or not, are not precluded by these observations, but, for reasons outlined above, regions of ER representing these other functions must be fairly small and/or in communication with RyR-rich regions.

The ER Is a Tunable Ca^{2+} Buffer that Retains a Record of Signaling Events

The companion article (see Albrecht et al., 2001, in this issue) introduced the concept that the particular complement of Ca^{2+} transport systems in a given cell specifies the availability of three distinct modes of CICR. One main experimental finding of the present study is that when $[Ca^{2+}]_i$ is maintained in the range ~600–800 nM, there is little net change in $[Ca]_{ER}$, suggesting that at these $[Ca^{2+}]_i$ levels, enhanced CICR via RyRs largely balances Ca^{2+} uptake, even though both inward and outward fluxes are larger than basal levels. Therefore, we conclude that sympathetic neurons express either Mode 2 or Mode 3 CICR, since these are the types characterized by a transition to net Ca^{2+} release.

After repolarization (from 50 K^+), $[Ca]_{ER}$ increased during the plateau phase of recovery, a period during which $[Ca^{2+}]_i$ is maintained at ~300 nM by net mitochondrial Ca^{2+} release (Pivovarova et al., 1999b; Colegrove et al., 2000). Since this is a permissive range for ER Ca^{2+} accumulation (see Albrecht et al., 2001, in this issue) the observation implies that Ca^{2+} release from mitochondria serves as a stimulus for ER Ca accumulation, thus, effectively determining which CICR mode is active. There is good evidence for stimulus-driven increases in $[Ca]_{ER}$ or $[Ca^{2+}]_{ER}$ in other neuronal cell types (Shmigol et al., 1994b; Markram et al., 1995; Garaschuk et al., 1997; Pozzo-Miller et al., 1997). One striking common feature of these increases is their longevity; recovery of $[Ca]_{ER}$ and/or $[Ca^{2+}]_{ER}$ to basal levels is extremely slow, typically on the order of tens of minutes. Long-lived changes in $[Ca]_{ER}$, with attendant effects on $[Ca^{2+}]_i$, would undoubtedly influence cellular processes, e.g., electrical excitability or synaptic activity, and, as mentioned, might be a mechanism for storing "memory traces" of previous activity over time frames suitable for processes like protein synthesis and transport. The longevity of $[Ca]_{ER}$ elevations also suggests future experiments directed toward understanding the extent to which the Ca load of the ER influences the mode and direction of ER Ca^{2+} transport.

The ER of sympathetic neurons appears to differ from certain other neuronal cell types in at least two important respects. First, the distribution of $[Ca]_{ER}$ measurements, at rest and in response to depolarization and a variety of drugs, is generally normal. Therefore, the results are consistent with the idea that the somatic ER of sympathetic neurons is a single functional entity, and provide no evidence for the existence of discrete ER domains that differ in their capacity to transport Ca^{2+}. Although this agrees with results from some nonmuscle cell types (Khodakhah and Armstrong, 1997), it contrasts with several others, (Golovina and Blaustein, 1997; Pozzo-Miller et al., 1997; for review see Meldolesi and Pozzan, 1998b). Second, the range of changes in $[Ca]_{ER}$ of sympathetic neurons, between 5 and 20 mmol/kg, is small, especially in comparison to the huge loads accumulated by, for example, the dendritic ER of CA3 pyramidal cells (Pozzo-Miller et al.,

1997). Taken together, these observations imply significant functional diversity of ER from one cell type (or region) to another, so that it remains a goal of future research to explain such heterogeneity, or lack thereof.

$[Ca^{2+}]_i$ Dependence of ER Ca^{2+} Transport Confers Location Dependence on the Transition from Ca^{2+} Sink to Source

Given the acceleration of ER Ca^{2+} release that occurs with stronger stimuli, we tested whether even larger $[Ca^{2+}]_i$ elevations lead to net ER Ca^{2+} release. After disabling mitochondrial Ca^{2+} uptake (with FCCP), the same strong depolarizing stimuli (50 mM K^+) raised $[Ca^{2+}]_i$ to >1 μM, with a concomitant decline in $[Ca]_{ER}$. This decline reflects Ca^{2+} release as expected during classical CICR, which, in turn, appears to have synergistically amplified the $[Ca^{2+}]_i$ response (Fig. 3 B) beyond that attributable to just Ca^{2+} entry.

It is increasingly clear that intracellular Ca^{2+} signaling depends on both time and space (Meldolesi and Pozzan, 1998a; Pozzan and Rizzuto, 2000). In sympathetic neurons, the spatial component is dominated by an initial Ca^{2+} flux across the plasma membrane, leading to pronounced radial gradients in $[Ca^{2+}]_i$ (Hernandez-Cruz et al., 1990; Hua et al., 1993b). Similar $[Ca^{2+}]_i$ gradients have been observed in several other cell types, including, for example, Purkinje cells (Eilers et al., 1995) and chromaffin cells (Neher and Augustine, 1992; Alonso et al., 1999). In view of the $[Ca^{2+}]_i$ dependence of CICR shown here, we asked whether transient gradients in $[Ca^{2+}]_i$ might influence the spatial profile of $[Ca]_{ER}$. In fact, a $[Ca]_{ER}$ gradient was observed at short times (10 s) during strong depolarization as a decline in $[Ca]_{ER}$ in the outermost shell adjacent to plasma membrane Ca^{2+} channels. A plausible explanation is that even though globally averaged $[Ca^{2+}]_i$ rises to only submicromolar levels, $[Ca^{2+}]_i$ just beneath the plasmalemma is high enough to drive CICR into the net release mode. We propose that this is another manifestation of the $[Ca^{2+}]_i$ dependence of net ER Ca^{2+} transport, and that triggered Ca^{2+} release from the ER can occur in the absence of drugs that modify Ca^{2+} homeostasis. Furthermore, this observation reveals that different modes of CICR can coexist in the same cell at the same time, potentially providing a driving force for directional intracisternal Ca^{2+} diffusion. Although the radial dependence of $[Ca]_{ER}$ may simply reflect the $[Ca^{2+}]_i$ dependence of CICR, there could well be additional factors. For example, recent reports (Akita and Kuba, 1999; McDonough et al., 2000) indicate that RyR's are preferentially expressed in the subplasmalemmal (and perinuclear) region of these cells. A spatial difference in the density of RyR's would undoubtedly affect, at least quantitatively, local expression of CICR (McDonough et al., 2000). Additionally, preferential depletion of peripherally placed cisterns would be an ideal spatial arrangement for activating store-operated channels (although there is presently no evidence for such channels in these neurons). Finally, we note again the likely possibility that the size of the preexisting ER Ca load influences stimulus-evoked changes in $[Ca]_{ER}$.

Spatiotemporal Interactions between the ER, Mitochondria, and Cytosolic Calcium

An important component of this study is the confirmation and quantitative refinement of the depolarization-induced radial gradient in $[Ca]_{mito}$. We previously reported such a gradient at 45 s after strong depolarization, but the EDX data underlying this analysis was scattered owing to the punctate distribution of mitochondrially sequestered Ca (Pivovarova et al., 1999a) and the point-probe nature of EDX analysis. Here, we report the shape and magnitude of this $[Ca]_{mito}$ gradient based on calcium maps obtained by EELSI (Leapman et al., 1994; Leapman and Rizzo, 1999). The refined EELSI profile of $[Ca]_{mito}$ versus distance from the plasmalemma (Fig. 5 B) presented here is consistent with previous results from these and other cells (Bito et al., 1996; Wang et al., 1999; Montero et al., 2000) and supports speculation that mitochondrial Ca loading, because of its steep dependence on $[Ca^{2+}]_i$, retains a spatial record of $[Ca^{2+}]_i$ gradients.

The cytoplasmic shell where maximal mitochondrial Ca^{2+} uptake occurs coincides with the shell of maximal ER Ca release. This and other observations—for example, the rapid $[Ca^{2+}]_i$ decline followed by a plateau seen after caffeine/ryanodine-evoked dumping of the ER Ca store (Fig. 2 C)—suggest functional coupling between these two organelles and are consistent with the idea of direct Ca transfer within organized, functional complexes (Rizzuto et al., 1994, 1998; Montero et al., 2000). However, they are also consistent with coupling through bulk cytosolic Ca^{2+}. Regardless of mechanistic details, it is clear that over a range of time, space, and $[Ca^{2+}]_i$, mitochondria and the ER engage in complementary Ca^{2+} transport, implying some degree of coupling. The functional consequences of such coupling are unknown, but could well be profound. As a specific example, the transformation of the ER into a triggered Ca^{2+} source when mitochondrial Ca^{2+} uptake is disabled suggests that mitochondria may be important regulators of CICR mode transitions. On a more general level, either or both organelles could serve as memory reservoirs for important functions such as synaptic potentiation or facilitation (Pozzo-Miller et al., 1997; Berridge, 1998; Zucker, 1999). Perhaps the ER and mitochondria share such functions, cooperating through overlapping, coordinated time domains within a common local spatial domain (Pozzo-Miller et al., 2000). If this occurs, it remains to be determined whether the ER senses mitochondrial

Ca^{2+} transport, and vice versa, through local or global mechanisms.

We thank Drs. T.S. Reese and E.S. Ralston for helpful discussions and critical evaluation and Dr. C.A. Brantner for excellent technical assistance.

This work was supported by a grant (No. NS-33514) from the NIH to D.D. Friel and by the NIH Intramural Research Program.

Received: 6 October 2000
Revised: 15 May 2001
Accepted: 17 May 2001

REFERENCES

Akita, T., and K. Kuba. 1999. Ca^{2+} release from the submembrane and perinuclear Ca^{2+} stores induced by action potentials and its modulation of the cell membrane excitability in cultured sympathetic neurons. *Soc. Neurosci.* 25:1990. (Abstr.)

Alonso, M.T., M.J. Barrero, P. Michelena, E. Carnicero, I. Cuchillo, A.G. Garcia, J. Garcia-Sancho, M. Montero, and J. Alvarez. 1999. Ca^{2+}-induced Ca^{2+} release in chromaffin cells seen from inside the ER with targeted aequorin. *J. Cell. Biol.* 144:241–254.

Albrecht, M.A., S.L. Colegrove, J. Hongpaisan, N.B. Pivovarova, S.B. Andrews, and D.D. Friel. 2001. Activation of a Ca^{2+}-induced Ca^{2+} release pathway attenuates ER Ca^{2+} accumulation in sympathetic neurons. *J. Gen. Physiol.* 118:83–100.

Berridge, M.J. 1998. Neuronal calcium signaling. *Neuron.* 21:13–26.

Bito, H., K. Deisseroth, and R.W. Tsien. 1996. CREB phosphorylation and dephosphorylation: a Ca^{2+}- and stimulus duration-dependent switch for hippocampal gene expression. *Cell.* 87:1203–1214.

Buchanan, R.A., R.D. Leapman, M.F. O'Connell, T.S. Reese, and S.B. Andrews. 1993. Quantitative scanning transmission electron microscopy of ultrathin cryosections: subcellular organelles in rapidly frozen liver and cerebellar cortex. *J. Struct. Biol.* 110:244–255.

Colegrove, S.L., M.A. Albrecht, and D.D. Friel. 2000. Dissection of mitochondrial Ca^{2+} uptake and release fluxes in situ after depolarization-evoked $[Ca^{2+}]_i$ elevations in sympathetic neurons. *J. Gen. Physiol.* 115:351–370.

Cseresnyés, Z., A.I. Bustamente, M.G. Klein, and M.F. Schneider. 1997. Release-activated Ca^{2+} transport in neurons of frog sympathetic ganglia. *Neuron.* 19:403–419.

David, G. 1999. Mitochondrial clearance of cytosolic Ca^{2+} in stimulated lizard motor nerve terminals proceeds without progressive elevation of mitochondrial matrix $[Ca^{2+}]$. *J. Neurosci.* 19:7495–7506.

Eilers, J., G. Callewaert, C. Armstrong, and A. Konnerth. 1995. Calcium signaling in a narrow somatic submembrane shell during synaptic activity in cerebellar Purkinje neurons. *Proc. Natl. Acad. Sci. USA.* 92:10272–10276.

Emptage, N., T.V. Bliss, and A. Fine. 1999. Single synaptic events evoke NMDA receptor-mediated release of calcium from internal stores in hippocampal dendritic spines. *Neuron.* 22:115–124.

Friel, D.D. 1995. $[Ca^{2+}]_i$ oscillations in sympathetic neurons: an experimental test of a theoretical model. *Biophys. J.* 68:1752–1766.

Friel, D.D., and R.W. Tsien. 1992. A caffeine- and ryanodine-sensitive Ca^{2+} store in bullfrog sympathetic neurones modulates effects of Ca^{2+} entry on $[Ca^{2+}]_i$. *J. Physiol.* 450:217–246.

Garlid, K.D., and R.A. Nakashima. 1983. Studies on the mechanism of uncoupling by amine local anesthetics. Evidence for mitochondrial proton transport mediated by lipophilic ion pairs. *J. Biol. Chem.* 258:7974–7980.

Garaschuk, O., Y. Yaari, and A. Konnerth. 1997. Release and sequestration of calcium by ryanodine-sensitive stores in rat hippocampal neurones. *J. Physiol.* 502:13–30.

Golovina, V.A., and M.P. Blaustein. 1997. Spatially and functionally distinct Ca^{2+} stores in sarcoplasmic and endoplasmic reticulum. *Science.* 275:1643–1648.

Hernandez-Cruz, A., F. Sala, and P.R. Adams. 1990. Subcellular calcium transients visualized by confocal microscopy in a voltage-clamped vertebrate neuron. *Science.* 247:858–862.

Holm, S. 1979. A simple sequentially rejective multiple test procedure. *Scand. J. Statist.* 6:65–70.

Hua, S.Y., K. Kuba, and M. Nohmi. 1993a. Excitation-induced Ca^{2+} dynamics in sympathetic neurons measured with conventional epifluorescence and confocal UV laser-scanning microscopes. *Jpn. J. Physiol.* 43:S153–S160.

Hua, S.Y., M. Nohmi, and K. Kuba. 1993b. Characteristics of Ca^{2+} release induced by Ca^{2+} influx in cultured bullfrog sympathetic neurones. *J. Physiol.* 464:245–272.

Hunt, J.A., G. Kothleitner, and R. Harmon. 1999. Comparison of STEM EELS spectrum-imaging vs. EFTEM spectrum-imaging. *Microsc. Microanal.* 5(*Suppl.*):616-617.

Khodakhah, K., and C.M. Armstrong. 1997. Inositol trisphosphate and ryanodine receptors share a common functional Ca^{2+} pool in cerebellar Purkinje neurons. *Biophys. J.* 73:3349–3357.

Kuba, K. 1994. Ca^{2+}-induced Ca^{2+} release in neurones. *Jpn. J. Physiol.* 44:613–650.

Kuba, K., and S. Nishi. 1976. Rhythmic hyperpolarizations and depolarization of sympathetic ganglion cells induced by caffeine. *J. Neurophysiol.* 39:547–563.

Leapman, R.D., J.A. Hunt, R.A. Buchanan, and S.B. Andrews. 1993. Measurement of low calcium concentrations in cryosectioned cells by parallel-EELS mapping. *Ultramicroscopy.* 49:225–234.

Leapman, R.D., and N.W. Rizzo. 1999. Towards single atom analysis of biological structures. *Ultramicroscopy.* 78:251–268.

Leapman, R.D., S.Q. Sun, J.A. Hunt, and S.B. Andrews. 1994. Biological electron energy loss spectroscopy in the field-emission scanning transmission electron microscope. *Scanning Microsc.* 8(*Suppl.*):245–258.

Lipscombe, D., D.V. Madison, M. Poenie, H. Reuter, R.W. Tsien, and R.Y. Tsien. 1988. Imaging of cytosolic Ca^{2+} transients arising from Ca^{2+} stores and Ca^{2+} channels in sympathetic neurons. *Neuron.* 1:355–365.

Markram, H., P.J. Helm, and B. Sakmann. 1995. Dendritic calcium transients evoked by single back-propagating action potentials in rat neocortical pyramidal neurons. *J. Physiol.* 485:1–20.

McDonough, S.I., Z. Cseresnyés, and M.F. Schneider. 2000. Origin sites of calcium release and calcium oscillations in frog sympathetic neurons. *J. Neurosci.* 20:9059–9070.

Meldolesi, J., and T. Pozzan. 1998a. The endoplasmic reticulum Ca^{2+} store: a view from the lumen. *Trends Biochem. Sci.* 23:10–14.

Meldolesi, J., and T. Pozzan. 1998b. The heterogeneity of ER Ca^{2+} stores has a key role in nonmuscle cell signaling and function. *J. Cell Biol.* 142:1395–1398.

Minamikawa, T., D.A. Williams, D.N. Bowser, and P. Nagley. 1999. Mitochondrial permeability transition and swelling can occur reversibly without inducing death in intact human cells. *Exp. Cell Res.* 246:26–37.

Montero, M., M.T. Alonso, E. Carnicero, I. Cuchillo-Ibanez, A. Albillos, A.G. Garcia, J. Garcia-Sancho, and J. Alvarez. 2000. Chromaffin-cell stimulation triggers fast millimolar mitochondrial Ca^{+} transients that modulate secretion. *Nat. Cell Biol.* 2:57–61.

Neher, E., and G.J. Augustine. 1992. Calcium gradients and buffers in bovine chromaffin cells. *J. Physiol.* 450:273–301.

Petronilli, V., C. Cola, S. Massari, R. Colonna, and P. Bernardi. 1993. Physiological effectors modify voltage sensing by the cyclosporin A-sensitive permeability transition pore of mitochondria. *J. Biol. Chem.* 268:21939–21945.

Pfaffinger, P.J., M.D. Leibowitz, E.M. Subers, N.M. Nathanson, W. Almers, and B. Hille. 1988. Agonists that suppress M-current

elicit phosphoinositide turnover and Ca^{2+} transients, but these events do not explain M-current suppression. *Neuron.* 1:477–484.

Pivovarova, N.B., J. Hongpaisan, S.B. Andrews, and D.D. Friel. 1999a. Depolarization-induced mitochondrial Ca accumulation in sympathetic neurons: spatial and temporal characteristics. *J. Neurosci.* 19:6372–6384.

Pivovarova, N.B., J. Hongpaisan, D.D. Friel, R.D. Leapman, and S.B. Andrews. 1999b. Intra- and intermitochondrial Ca heterogeneity induced by calcium entry in sympathetic neurons. *Soc. Neurosci.* 25:1249. (Abstr.)

Pozzan, T., and R. Rizzuto. 2000. High tide of calcium in mitochondria. *Nat. Cell Biol.* 2:E25–E27.

Pozzan, T., R. Rizzuto, P. Volpe, and J. Meldolesi. 1994. Molecular and cellular physiology of intracellular calcium stores. *Physiol. Rev.* 74:595–636.

Pozzo-Miller, L.D., J.A. Connor, and S.B. Andrews. 2000. Microheterogeneity of calcium signalling in dendrites. *J. Physiol.* 525:53–61.

Pozzo-Miller, L.D., N.B. Pivovarova, R.D. Leapman, R.A. Buchanan, T.S. Reese, and S.B. Andrews. 1997. Activity-dependent calcium sequestration in dendrites of hippocampal neurons in brain slices. *J. Neurosci.* 17:8729–8738.

Rizzuto, R., C. Bastianutto, M. Brini, M. Murgia, and T. Pozzan. 1994. Mitochondrial Ca^{2+} homeostasis in intact cells. *J. Cell Biol.* 126:1183–1194.

Rizzuto, R., P. Pinton, W. Carrington, F.S. Fay, K.E. Fogarty, L.M. Lifshitz, R.A. Tuft, and T. Pozzan. 1998. Close contacts with the endoplasmic reticulum as determinants of mitochondrial Ca^{2+} responses. *Science.* 280:1763–1766.

Sandler, V.M., and J.G. Barbara. 1999. Calcium-induced calcium release contributes to action potential-evoked calcium transients in hippocampal CA1 pyramidal neurons. *J. Neurosci.* 19:4325–4336.

Shmigol, A., S. Kirischuk, P. Kostyuk, and A. Verkhratsky. 1994a. Different properties of caffeine-sensitive Ca^{2+} stores in peripheral and central mammalian neurones. *Pflügers Arch.* 426:174–176.

Shmigol, A., P. Kostyuk, and A. Verkhratsky. 1994b. Role of caffeine-sensitive Ca^{2+} stores in Ca^{2+} signal termination in adult mouse DRG neurones. *Neuroreport.* 5:2073–2076.

Shmigol, A., A. Verkhratsky, and G. Isenberg. 1995. Calcium-induced calcium release in rat sensory neurons. *J. Physiol.* 489:627–636.

Stout, A.K., H.M. Raphael, B.I. Kanterewicz, E. Klann, and I.J. Reynolds. 1998. Glutamate-induced neuron death requires mitochondrial calcium uptake. *Nat. Neurosci.* 1:366–373.

Thayer, S.A., L.D. Hirning, and R.J. Miller. 1988. The role of caffeine-sensitive calcium stores in the regulation of the intracellular free calcium concentration in rat sympathetic neurons in vitro. *Mol. Pharmacol.* 34:664–673.

Usachev, Y.M., and S.A. Thayer. 1999. Controlling the urge for a Ca^{2+} surge: all-or-none Ca^{2+} release in neurons. *Bioessays.* 21:743–750.

Verkhratsky, A., and A. Shmigol. 1996. Calcium-induced calcium release in neurones. *Cell Calcium.* 19:1–14.

Verkhratsky, A.J., and O.H. Petersen. 1998. Neuronal calcium stores. *Cell Calcium.* 24:333–343.

Wang, G.J., K. Baron, and S.A. Thayer. 1999. NMDA-induced intramitochondrial calcium changes in hippocampal neurons in culture. *Soc. Neurosci.* 25:1603. (Abstr.)

Zucker, R.S. 1999. Calcium- and activity-dependent synaptic plasticity. *Curr. Opin. Neurobiol.* 9:305–313.